Microporous and Mesoporous Materials 325 (2021) 111316

Contents lists available at ScienceDirect

Microporous and Mesoporous Materials

journal homepage: www.elsevier.com/locate/micromeso

Biocomposites based on SBA-15 and papain: Characterization, enzymatic activity and cytotoxicity evaluation

Danilo W. Losito [a], Patricia S. Lopes [b], Andreza R. Ueoka [b], Márcia C.A. Fantini [c], Pedro Leonidas Oseliero Filho [c], Newton Andréo-Filho [d], Tereza S. Martins [a,*]

[a] Laboratório de Materiais Híbridos, Instituto de Ciências Ambientais, Químicas e Farmacêuticas. Universidade Federal de São Paulo, Diadema, SP, Brazil
[b] Laboratório de Imunologia Celular & Bioquímica de fungos e protozoários (LICBfp), Instituto de Ciências Ambientais, Químicas e Farmacêuticas. Universidade Federal de São Paulo, Diadema, SP, Brazil
[c] Instituto de Física, Universidade de São Paulo, São Paulo, SP, Brazil
[d] Laboratório de Farmacotécnica e Cosmetologia, Instituto de Ciências Ambientais, Químicas e Farmacêuticas. Universidade Federal de São Paulo, Diadema, SP, Brazil

ARTICLE INFO

Keywords:
Biocomposites
Ordered mesoporous silica
Papain
Biological activity
Spheroids cytotoxicity

ABSTRACT

Papain has bacteriostatic and anti-inflammatory properties and has been shown to be effective in the healing process of wounds, injuries, and ulcers by breaking down fibrinous material into necrotic tissue. However, papain is unstable and easily denatures or deactivates preventing their broad industrial application. In this work, papain was incorporated into SBA-15 ordered mesoporous silica, with the aim of improving its stability, as well as its encapsulation yield and influence of the reaction time on its stability and enzymatic activity. By small-angle X-ray scattering it was possible to verify that the papain is a globular and slightly elongated protein, likely dimeric, with a maximum size of ~6.0 nm, which favors its inclusion in the SBA-15 mesopores (~10 nm). The biocomposites (SBA-15:papain) were characterized by several physical-chemical techniques. The results indicated that the papain was incorporated into the SBA-15 mesopores. The biocomposites exhibited higher thermal degradation temperature than pure papain and did not show cytotoxic potential. The papain enzymatic activity was maintained, with the best performance for the samples prepared with 30 wt% of papain. The results also showed that the 3D cell culture system is better suited for biocomposites that present a cell disruption mechanism.

1. Introduction

Papain is one of the most studied proteolytic enzymes of the cysteine proteinases group, extracted from the latex of the Carica papaya fruit, it was the first enzyme whose three-dimensional structure has been determined [1]. As a cysteine protease with a thiol group (SH) at its active site, it is an excellent structural model for this group of enzymes [2]. It has properties such as high enzymatic activity, good thermal stability and non-toxicity which allow a wide range of applications in the food, cosmetic, pharmaceutical and textile industries [3–5]. Papain has bacteriostatic and anti-inflammatory properties and has been shown to be effective in the healing process of wounds, injuries, and ulcers by breaking down fibrinous material into necrotic tissue [6]. However, papain is unstable and easily denatures or deactivates, such as other soluble enzymes, making them more difficult to recycle and recovery, preventing their broad industrial application. Aiming to overcome these limitations, immobilization of free enzymes is an effective way to solve them [7,8].

Enzymatic immobilization refers to enzymes physically confined to a matrix, maintaining their enzymatic activity, and increasing their stability [9–11]. Enzyme stability can be improved by reducing the autolysis in the case of protease enzymes, and the reduction of protein aggregation because of separation of adsorbed enzyme molecules in the surface [12]. Recently several techniques such as physical adsorption, entrapment, ion exchange and covalent bonding have been adopted to immobilize enzymes on solid supports, such as polyelectrophilic capsules, biopolymers, zeolites, and silicas such as mesoporous silicas [9, 11–15].

Ordered mesoporous silicas, such as MCM-41, SBA-15 and FDU-12, have several properties that make them attractive for enzymes

* Corresponding author. Department of Chemistry, Federal University of São Paulo (UNIFESP), Rua São Nicolau, 210, 2o andar, Diadema, São Paulo, CEP 09913-030, Brazil. Tel.: +55-11-40440500 R 3568.
E-mail address: tsmartins@unifesp.br (T.S. Martins).

https://doi.org/10.1016/j.micromeso.2021.111316
Received 10 April 2021; Received in revised form 15 July 2021; Accepted 19 July 2021
Available online 31 July 2021
1387-1811/

immobilization, such as uniform and tunable pores (2–50 nm), high surface area (above 800 $m^2\ g^{-1}$) and large number of silanol groups (Si–OH) which are important for grafting enzymes to the silica surface [12,16,17]. Various of these silicas have been used for enzyme immobilization [9,12,18,19], but among them, the SBA-15 is particularly promising as host matrix for papain immobilization due to its excellent structural properties, such as, highly ordered hexagonal, large and adjustable mesopores (8–50 nm) and high thermal and mechanical stability as a result of large silica wall thickness [20,21].

In this work, unlike other published studies [9,22,23], papain was immobilized on pristine SBA-15 by wetness impregnation [22], in deionized water, varying the amount of papain (10 and 30 wt%), at different reaction time (30 and 60 min). The study was targeted to examine the papain content and the influence of the reaction time on both, stability, and papain enzymatic activity, maintaining the safety of the material regarding cellular viability, aiming biomedical applications. As far as our knowledge, the simple procedure to prepare biocomposites of pristine SBA-15 and enzymes, using impregnation in pure aqueous medium, has not been explored. Aqueous medium is particularly interesting since there are no other molecules to interact and compete with papain for the free pores inside the porous matrix. Papain has its isoelectric point around 8.3, consequently, in water, the enzyme shows positive charge, making favorable its interaction with silanol groups in SBA-15, which are electronically negative. These interactions could be impaired with other negative species present in the medium. This could take place when salts, such as phosphate salts, are used as buffering compound. Furthermore, the use of buffering agents, like phosphate buffered saline (PBS), could significantly increase the final weight, if the final dispersion would be freeze-dried without any sample treatment, as dialysis, to eliminate the buffer salts. Furthermore, in this study we present an unprecedented analysis on the cytotoxicity of silica-papain-based biocomposites using a 3D spheroid method [24,25]. Cells grown as spheroids better simulate *in vivo* cell biology, so the use of 3D spheroids to assess the toxicity of the biocomposites of SBA-15 and papain is a novelty per se, and better resemble the *in vivo* situation. In addition, papain is a protease and presents an anoikis effect, a fact that difficult the evaluation of *in vitro* tests.

2. Experimental

2.1. Material

Tetraethylorthosilicate (TEOS, 98%, Sigma-Aldrich), poly(ethylene oxide)–poly(propylene oxide)–poly(ethylene oxide) (Pluronic P123®, $PEO_{20}PPO_{70}PEO_{20}$, Sigma-Aldrich, Brazil), hydrochloric acid (HCl, 37%, Synth, Brazil), nitric acid, HNO_3, (Sigma Aldrich), silver nitrate, $AgNO_3$, (Synth, Brazil), Deionized water, Nα- Benzoyl-DL-arginine p-nitroanilide hydrochloride (Sigma-Aldrich®, St Louis, USA), Sodium phosphate dibasic heptahydrate P.A. (Synth, Diadema, Brazil), Disodium ethylenediaminetetraacetate dihydrate P.A. (Synth, Diadema, Brazil), L-cysteine hydrochloride P.A. (Synth, Diadema, Brazil) Papain from *Carica papaya* (30000 USP-U/mg, EMD Chemicals Inc, San Diego, USA), Papain pharmaceutical grade (30000 USP-U/mg stabilized with sodium disulfite, Emprove® Essential Merck, Darmstadt, Germany), Glacial acetic acid (Synth, Diadema, Brazil). Dulbecco's Modified Eagle Medium (DMEM), fetal bovine serum (FBS), penicillin-streptomycin, L-glutamine and trypsin with EDTA were purchased from Vitrocell® (Campinas, Brazil), *Balb/c 3T3* (*clone A31*) mouse embryo *cells* (ATCC® CCL-163™) *was purchased from ATCC (American Tissue Culture Collection, Manassas, VA), NanoshuttlesTM and the Bio-Assembler SystemTM were purchased from n3D Biosciences, Inc. (Houston, TX),* 1-(4,5-Dimethylthiazol-2-yl)-3,5-diphenylformazan, Thiazolyl blue formazan (MTT) and dimethyl sulfoxide (DMSO) were purchased from Sigma Aldrich (St. Louis, MO) and PrestoBlue™ was purchased from Life Technologies Poland (Warsaw, Poland).

2.2. SBA-15 synthesis

SBA-15 was synthesized according to Zhao et al. [17], with a slight modification. 4 g of Pluronic P123® was dissolved in 120 mL of HCl (2 mol L-1) solution and 30 mL of deionized water and the mixture was kept under magnetic stirring for 1 h. Then, 8.9 mL of TEOS was added to the solution, which was continuously stirred for 24 h at 50 °C. The reaction mixture resulting was then placed in a Teflon-lined autoclave followed by hydrothermal treatment at 100 °C for 48 h. The precipitate obtained was filtered and washed with deionized water to remove chloride ions and after the solid was dried overnight at 60 °C. The template removal procedure was combining solvent extraction using ethanol at room temperature and calcination. After the extraction solvent procedure, the material was calcined at 540 °C under air atmosphere for 4 h. We have adopted the solvent extraction procedure [16], using ethanol as solvent, in order to recover and reuse the polymer Pluronic P123. Since it cannot be completely removed by this approach, the following calcination step is still necessary. However, because the remaining amount of polymer is small, the calcination procedure can be faster than it would be without solvent extraction. Moreover, the use of solvent extraction prior to calcination is recommended because it is a mild process of template removal, preserving the ordered porous structure.

2.3. Papain incorporation

The papain was dissolved in deionized water, then mixed with SBA-15, at the weight ratio of 1SBA-15:0.1PPN:33H_2O and 1SBA-15:0.3PPN:33H_2O. The obtained dispersion (pH = 5.3) was stirred at room temperature for 30 or 60 min and then it was frozen in a freezer at (−25 ± 5) °C for 24 h and after lyophilized at −52 °C, under vacuum (35 μmHg), for 48 h in a Liobras freeze-dryer (model Liotop® L108, São Carlos, Brazil). The resulting samples were referred as SBAPPNXa and SBAPPNXb, where SBA = SBA-15, PPN = papain, X = 10 or 30 wt% of papain and a = 60 min and b = 30 min of stirring.

2.4. Characterization

All samples were characterized by small-angle X-ray scattering (SAXS) performed on a Nanostar (Bruker) instrument equipped with a microfocus Genix 3D system (Xenocs) and a Vantec 2000 (Bruker) detector. The sample-to-detector distance was ~667 mm, which provided an effective range of the modulus of the transfer moment vector, $q = [4\pi \sin(\theta)]/\lambda$ (where 2θ is the scattering angle and $\lambda = 1.5418$ Å is the X-ray wavelength), experimentally accessible from 0.01 to 0.35 $Å^{-1}$. Both papain suspension (at concentration 3.5 mg mL^{-1}) and deionized water (used in the preparation of papain sample), were filled into reusable quartz capillaries with 1.5 mm in diameter mounted on stainless steel cases. The SBA-15:papain powder samples were placed in a sample holder between mica sheets. All measurements were performed at room temperature, RT = (22 ± 2) °C, and the data treatment, which includes azimuthal integration, background subtraction and absolute scale normalization, was performed using XSACT software supplied by Xenocs.

Dynamic light scattering (DLS) measurement of the same protein suspension sample was performed, at room temperature, on a Brookhaven DM-5000 Particle Size Analyzer, using a wavelength of 635 nm.

Nitrogen adsorption/desorption isotherms (NAI) were recorded on NOVA 1200e, Quantachrome Instruments. The samples were outgassed at 60 °C for 7 h and the isotherms were obtained at −196.15 °C using N_2 of 99.9998% purity and performed in the relative pressure range of 10^{-6} to 0.99 P/P_0. Pore size distribution curves and pore volume (V_{BJH}) were obtained using the Barrett-Joyner-Halenda (BJH) method [26] and the pore diameter (D_{pore}) was obtained from the maximum of the pore size distribution curve. The total pore volume (V_t) was estimated from the amount adsorbed at $P/P_0 = 0.99$. The specific surface area (S_{BET}) was

calculated using the Barrett-Emmett-Teller (BET) method [27] in the relative pressure P/P_0 range of 0.05–0.3 and the C-values were obtained from BET analysis.

SEM images were recorded on a JEOL microscope, model JSM 6610LV, operating with a secondary electron imaging (SEI) detector. The samples were placed onto conductive double-sided adhesive carbon tape and covered with a thin layer of gold.

Fourier transform infrared spectroscopy (FTIR) spectra were recorded on Agilent Cary 630 FTIR spectrometer, in the wavenumber range from 4000 to 400 cm^{-1}, using attenuated total reflectance (ATR) sample accessory.

Differential scanning calorimetry (DSC) and thermogravimetric analysis (TGA) measurements were performed using a simultaneous thermal analyzer DSC/TGA, the Discovery SDT 650 from TA Instruments. DSC/TGA curves were obtained at heating rate of 10 °C min^{-1}, in the temperature range from 35 °C to 900 °C, under dynamic air atmosphere (100 mL min^{-1}), using alumina crucible with ca. 5 mg of the sample mass.

Carbon, hydrogen, nitrogen, and sulfur (CHNS) were determined by microanalytical procedures, using a Thermo Scientific FlashEA™ 1112 HT Elemental Analyzer (Thermo Fisher Scientific).

2.5. Enzyme activity assay

The proteolytic activity of papain was determined by spectrophotometric method by measuring the rate at which p-nitroaniline was released at 405 nm. p-nitroaniline, a yellow substance, was produced by hydrolysis reaction of Na-benzoyl-DL-arginine p-nitroanilide hydrochloride (BAPA) (Sigma-Aldrich®, USA), a specific substrate to proteolytic enzymes as papain [28–30]. For that, an analytical curve to quantify the papain activity was built relating the rates of BAPA conversion and the papain concentrations. The rates of BAPA conversion were determined through relationship between absorbance at 405 nm of BAPA hydrolysis reaction product and reaction time (zero, 15, 30 and 45 min), for eight different papain concentrations. Initially, solutions of BAPA (880 μg mL^{-1}), acetic acid (30% v/v) and cysteine-phosphate buffer solutions, pH 6.8, containing papain ranging 0.0090–0.1090 mg mL^{-1} were prepared for immediate use. For the test, one 96-well plate was prepared with reagents in ice-bath to avoid that reaction starts. Each well enclosed 125 μL of BAPA solution and 100 μL of papain solutions in different concentrations for the four reaction times. For wells related to zero-time reaction 50 μL acetic acid was added before the plate was taken to a heated bath at 40 °C and starting to count the time. Acetic acid solution (50 μL) also was added to corresponding wells in 15, 30 and 45 min to stop the reaction. The same plate was used for reading the BAPA reaction product in a spectrophotometer at $\lambda = 405$ nm on a Synergy HT microplate reader (Biotek Instruments, USA) [31]. The absorbance values were recorded and related to reaction time making possible to determine the rate of BAPA conversion for each papain concentration. The linear relation between rates of BAPA conversion and papain concentration allows determining the equivalent concentration in active papain for a sample with unknown enzyme concentration.

The tests for SBAPPN biocomposites were performed weighting an amount of SBAPPN necessary to reach 1.0 mg papain in the composite. Thus, 10 mg of SBAPPN10 or 3.3 mg of SBAPPN30 were weighted and dispersed in 4 mL of cysteine-phosphate buffer pH 6.8, resulting in theoretical papain concentration of 0.250 mg mL^{-1}. These dispersions were directly used to evaluate the papain activity in BAPA substrate specific method. For that, 100 μL dispersions were immediately taken after homogenization and transferred to a 96-wells plate. The experiment was carried out as described to build the analytical curve for papain activity. The theoretical concentration of PPN in each well was 0.09 mg mL^{-1}. All the experiments were done in triplicate.

The BAPA conversion rates for the reaction products were determined by the relation between absorbance of reaction products at 405 nm and time. The concentration of papain in SBAPPN biocomposites was determined applying those rates in the analytical curve of papain concentration *vs* conversion rates. The percentage of biological activity retained in SBAPPN biocomposites was obtained by the ratio between concentration of PPN-determined and the theoretical papain concentration.

Since the SBA-15 is not soluble in aqueous media, after reading in the spectrophotometer, the plate was submitted to centrifugation to separate any suspended material, and it was read again at 405 nm. This procedure was performed to verify if there was any interference with the suspended material in the analysis.

2.6. Leaching test of immobilized papain on SBA-15

The SBAPPN30a biocomposite that showed an indicative of greatest amount of papain inside the mesopores was chosen for the leaching test of immobilized papain on SBA-15. The test was performed under stirring in aqueous solution. For this, 4.0 mg of composite were weighed and dispersed in 10 mL water in glass bottles. The dispersions were kept under magnetic stirring for 1, 2, 4, and 8 h at room temperature. In each time, the dispersions were filtered in nylon membrane (0.22 μm pore) discarding the firsts 4.0 mL for filter saturation. The next 4.0 mL filtered were collected and analysed in spectrophotometer (Thermo, Evolution 201, Brazil) in the wavelength range from 200 to 400 nm. A sample only containing SBA-15 was performed with the same procedure and used as a blank for the measurements. The equipment was baselined with purified water. The pH of the filtered samples were measured after the leaching assays. All analyses were done in triplicate. The data of absorbance were applied in an analytical curve for PPN in water ranging from 0.016 to 0.510 mg mL^{-1}, obtained as described by Nambu et al. [32] for determination of the PPN concentration, allowing to estimate the amount of PPN leached with time. The data obtained in different times were compared using One-Way ANOVA at a level of significance of 0.05.

2.7. Cytotoxicity assay using a 3D spheroid method

Balb/c 3T3 murine fibroblasts cells were cultured in DMEM with 10% FBS, 1% L-glutamine and 1% penicillin-streptomycin at 37 °C in 5% CO_2 conditions for both 2D and 3D cultures.

To perform the 3D *in vitro* test, the Bio-Assemble^{rTM} System (in 96-well configuration) from n3D Biosciences, Inc (Houston, TX, USA) was used to construct the 3D *in vitro* fibroblast spheroids. The assembly of 3D *in vitro* cultures was performed as previously reported [24,25,33] with a small adaptation using the protocol for suspension cells. Briefly, after the fibroblast culture cells in 2D reach ~80% confluence, the medium was aspirated; the culture flask was washed once with phosphate buffer solution. Then the cell detachment was done by incubation the cells with tripsin-EDTA solution for 5 min. The culture medium was added to stop the tripsin-EDTA action; the cells were centrifuged at 1500 rpm for 5 min; the supernatant was aspirated, and the pellet was re-suspended in culture medium. The number of cells in suspension was counted using a hemocytometer. After that, the cell suspension concentration of 5×10^4 cells/spheroid and the NanoShutlle™ at a concentration of 1 μL $mL^{-1} \times 10^4$ cells mL^{-1} were added into a centrifuged tube and the cells were centrifuged down at 1500 rpm for 5 min. The cell pellet was re-suspended using pipette action until the pellet to be well dispersed. The same procedure was repeated for two more times until the pellet reaches a homogeneous brown color. The supernatant was aspirated, and the cells were re-suspended in culture medium which was distributed into an ultra-low attachment 96-well plate (Greiner) at a concentration of 5×10^4 cells/well. Immediately afterwards, the plate was placed atop a magnetic drive of 96 neodymium magnets to attract the cells to form a spheroid. These spheroids were placed with the magnetic drive in the cell incubator for 24 h. In the next day, the magnetic drive was removed, and the cells were remodeling for 24 h. At this point, the

spheroids were ready to use.

After the formation of spheroids, the culture medium was removed and the cells were treated with SBA-15 (0.7 mg mL^{-1}), PPN (0.216 mg mL^{-1}), SBAPPN (1 mg mL^{-1}) and DMSO (200 mg mL^{-1}) for 24 h and the treatments were replaced with 10% MTT in cells media. All the materials presented concentrations that were equivalent between the free forms and complexed ones. The cells were incubated with the reagent for 2 h at 37 °C. Then, the media was aspirated, and the remaining formazan was dissolved in cold isopropanol and lysate by pipette action. The absorbance of the solution was then read at 570 nm in a spectrophotometer (Synergy HT Biotek, USA). Dose-response curves were plotted and fit to a Boltzmann sigmoidal function in GraphPad Prism 7 (GraphPad Software, La Jolla, CA, USA).

To compare the results, it was also performed a 3D PrestoBlue™ assay. After the formation of spheroids, the culture medium was removed and the cells were treated with SBA-15, papain, SBAPPN and DMSO for 24 h and the treatments were replaced with 1 X of PrestoBlue™ solution. The cells were incubated with the reagent for 2 h at 37 °C. Then, the cells were lysate by pipette action and the fluorescence of the solution was then read at 530 nm (excitation) and 590 (emission) in a spectrophotometer (Synergy HT Biotek, USA). Dose-response curves were plotted and fit to a Boltzmann sigmoidal function in GraphPad Prism 7 (GraphPad Software, La Jolla, CA, USA).

The results were analysed by calculations of means, standard deviation, and coefficient of variation. Subsequently, they were evaluated by multi-factor variance analysis (ANOVA) at a significance level of 95% ($\alpha = 0.05$). The results were submitted to the Tukey test, for significance analysis between the means, with the significance level of 1 and 5% or to the Sidak's multiple comparisons test with the significance level of 1 and 5%.

3. Results and discussion

3.1. SAXS

3.1.1. Papain

The obtained SAXS curve is shown in Fig. 1A (filled circles). The CRYSOL software [34] and the crystallographic structure of papain (9pap.pdb), shown in Fig. 1B, were used. It was observed a satisfactory agreement between the experimental data and the theoretical one (Fig. 1A, continuous line). The discrepancies, related to structural differences, are likely due to the thermal and hydration effects.

In order to estimate the size of papain in aqueous dispersion from SAXS measurements, the Indirect Fourier Transform (IFT) analysis [35] was performed, which provides information in real space. The result is depicted in Fig. 2. From the IFT fitting (Fig. 2A, continuous line) using WIFT software [36], the pair distance distribution function, *p(r)*, is obtained (Fig. 2B). The *p(r)* profile suggests that the protein has a globular and slightly elongated shape with longest length of ~6.0 nm (determined where $p(r) \approx 0$). The oscillation in the *p(r)* curve at r = 5.0 nm indicated a dimer-like form, in agreement with the correspondent crystallographic structure of papain (Fig. 1B). From IFT analysis the forward scattering, I(0) = (0.0628 ± 0.0004) cm^{-1}, and the protein radius of gyration, R_G = (1.97 ± 0.01) nm, were evaluated. The parameter I(0) is related to the protein molecular weight, M_W (in kDa), by (Oliveira 2011):

$$M_W = \frac{I(0)\cdot N_A}{c\cdot(\Delta\rho_m)^2}$$

where N_A is the Avogadro's number, c is the concentration of the protein (in mg mL^{-1}) and $\Delta\rho_m$ is the excess scattering length density per unit mass (in cm g^{-1}). A fair approximation of $\Delta\rho_m$ for proteins is 2×10^{10} cm g^{-1} [37]. Using $c = 3.5$ mg mL^{-1}, we will have $M_W \approx 27.1$ kDa. Since the expected value is 23.406 kDa [38], the obtained M_W is satisfactory, indicating a quite monodisperse sample.

The size of the protein in aqueous dispersion was also investigated using DLS. The measured correlation function $C(t)$ is shown in Fig. 3A (filled circles). By using the Non-Negatively constrained Least Squares (NNLS) method [39] to satisfactorily fit the $C(t)$ function, we obtained the histograms of hydrodynamic diameter per intensity (Fig. 3B), per volume (Fig. 3C) and per number of particles (Fig. 3D). As we can observe from the histogram of diameter per intensity (Fig. 3D), there are two populations with mean diameters of ~4.0 and ~60.0 nm (estimated to be the approximate center of the correspondent distributions). Despite the existence of the larger particles (likely protein aggregates), they are much less numerous according to the histograms of diameter per volume (Fig. 3C) and per number (Fig. 3D).

Using the HYDROPO software [40] as well as the crystallographic structure of papain (Fig. 1B), the predicted hydrodynamic diameter of this protein is ~4.7 nm, in agreement with the value obtained by DLS analysis. In addition, the estimated radius of gyration and the longest papain length are, respectively, ~1.7 and ~6.0 nm, also in agreement with the SAXS results.

3.1.2. SBA-15:papain (SBAPPN)

SAXS curves of SBA-15 and SBAPPN biocomposites are shown in Fig. 4A, where five diffraction peaks are indexed, which are

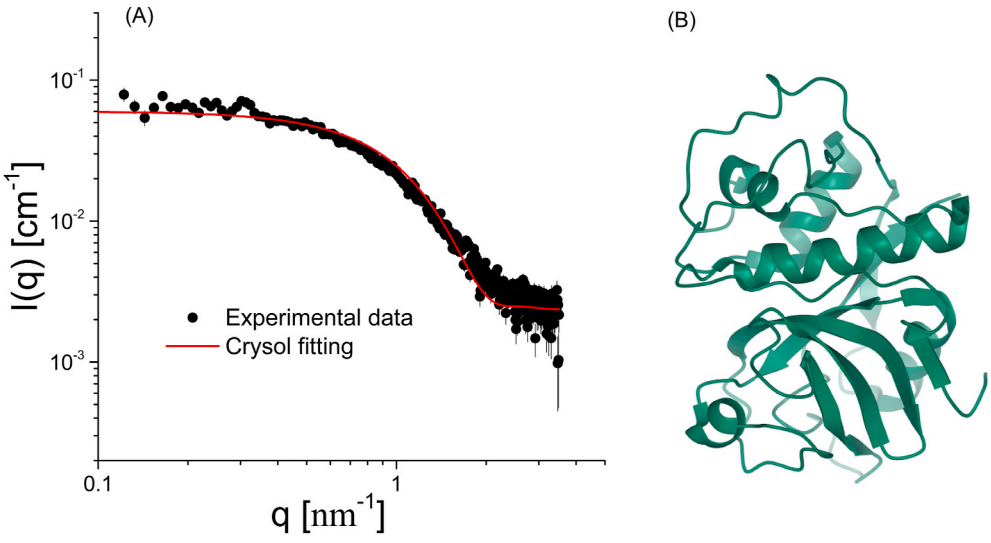

Fig. 1. A) Fitting of SAXS curve with CRYSOL software. B) Crystallographic structure of papain protein (9pap.pdb) used in CRYSOL analysis.

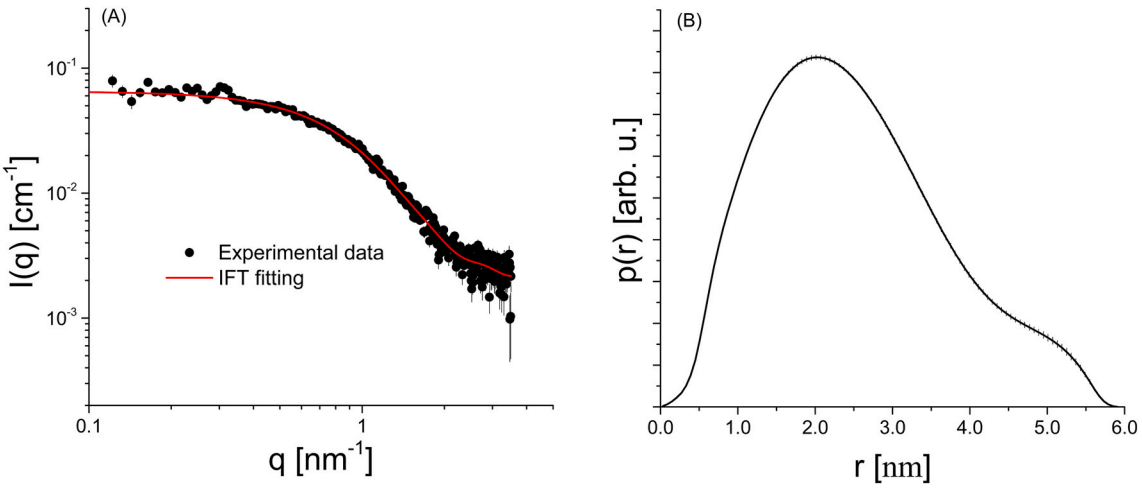

Fig. 2. A) Fitting of the SAXS curve with WIFT software. B) From the obtained p(r), whose profile is compatible with the fact that papain is a globular and slightly elongated protein with two domains (Fig. 1B), we conclude that the longest protein length is ~6.0 nm.

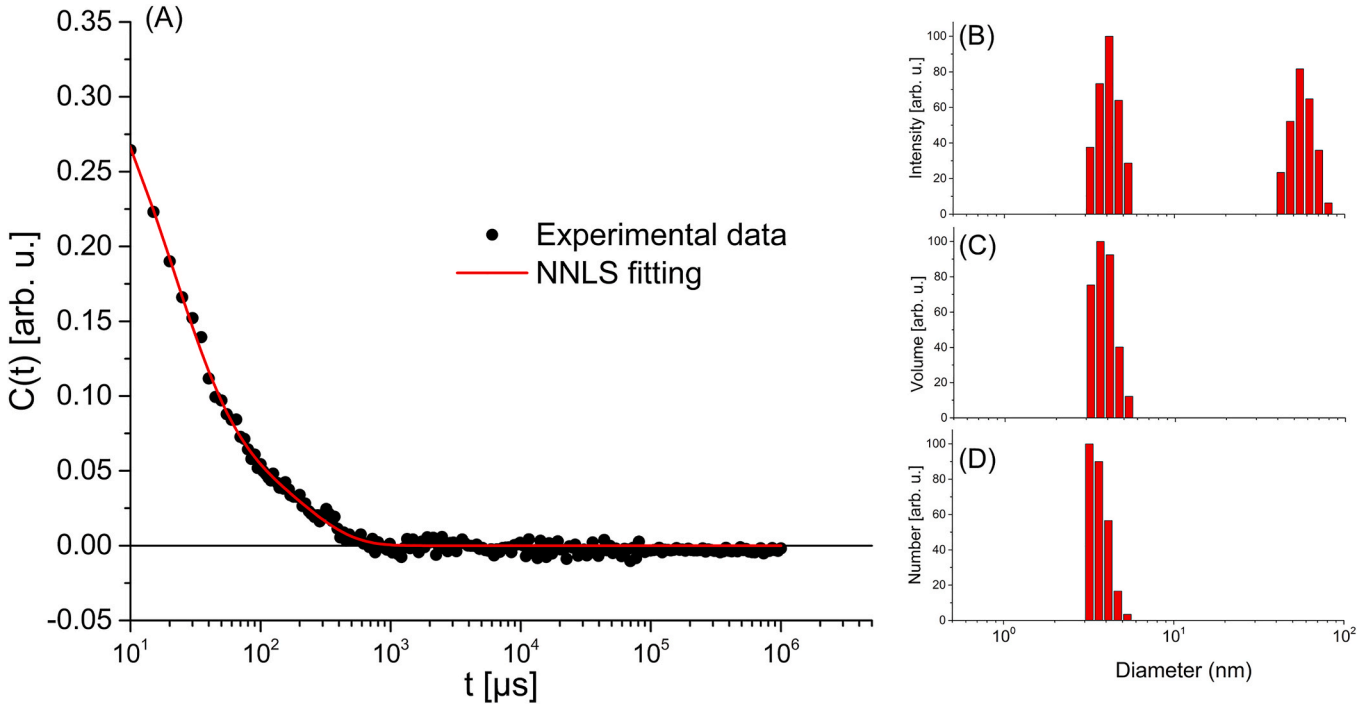

Fig. 3. A) Correlation function curve fitted by the NNLS method. From this analysis, the hydrodynamic diameter distributions of papain per intensity (B), volume (C) and number (D) were obtained.

characteristics of SBA-15 with a highly ordered 2D hexagonal mesostructure (space group *p6mm*) [41–43]. Free-modeling structural parameters (interplanar spacing, $d_{(hkl)}$ and lattice parameter ($a_{(hkl)}$), obtained from the peak indexation, are shown in Table 1. No significant changes in these parameters were observed, although the intensity of the diffraction peaks of SBAPPN biocomposites decreased compared to pure SBA-15, indicating the papain incorporation into the SBA-15 mesoporosity. However, as the reaction time increases (from 30 to 60 min) the reduction in intensity is more evident, suggesting that the reaction time may influence the amount of papain loaded into the SBA-15 mesopores as well as the formation of protein aggregates, located on the surface of the silica matrix, since large scattering amplitudes were observed at low q values for the samples with papain. The insert in Fig. 4A shows a zoom in the region from $q = 0.10$ Å^{-1} to 0.25 Å^{-1} to better visualization of the (110), (200), (210) and (300) reflections. In order to evaluate the presence of papain in the silica matrix, a theoretical model [44] was used to satisfactorily fit the experimental data (Fig. 4B). The fitting was performed considering only scale parameters, pore internal radius and wall thickness, and the obtained results are presented in Table 2. The internal radius is smaller for the samples containing papain, indicating its presence inside the mesoporosity. The slight increase on the wall thickness observed for the samples with papain compared to pure SBA-15 can be attributed to lyophilization or some impregnation of papain outside the silica tubes. On the other hand, the values of Scale and Backgr parameters suggest that higher times and papain concentrations lead to higher adsorption of the protein into the silica matrix, since Scale and Backgr have small values in these cases. In addition, according to the values of Scale_q^4 parameter, short periods of impregnation and high papain concentrations could be linked to indications of papain aggregation outside the mesopores, therefore

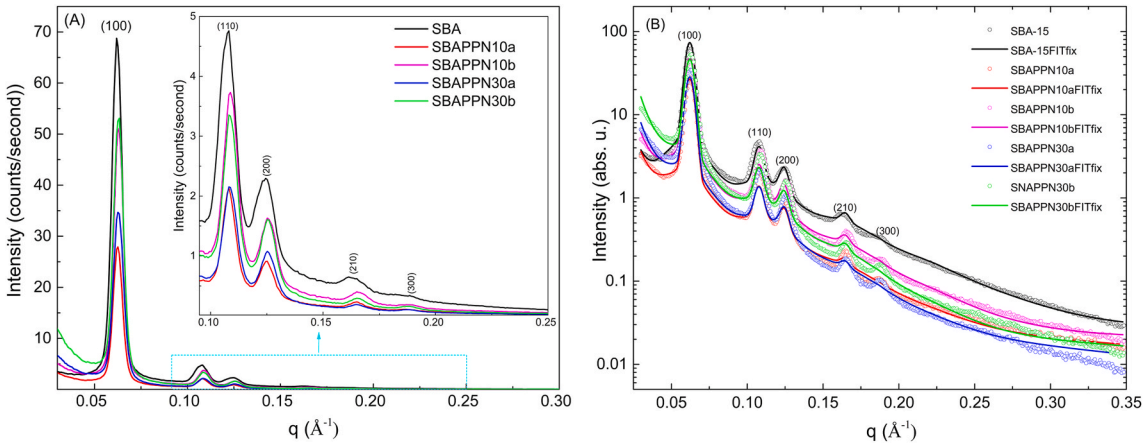

Fig. 4. (A) SAXS measurements of SBA-15 and SBAPPN biocomposites. (B) SAXS experimental data and fitting with the structural theoretical model of the samples.

Table 1
Structural and textural properties of SBA-15 and SBAPPN biocomposites obtained by NAI and free modeling SAXS analyses.

Samples	SAXS			NAI			
	$d_{(hkl)}/a_{(hkl)}$ (nm)			S_{BET} (m^2 g^{-1})/C-values	D_{pore} (nm)	V_{BJH}/V_t (cm^3 g^{-1})	Wt (nm)
	(100)	(110)	(200)				
SBA-15	10.1/11.7	5.8/11.6	5.0/11.6	832/249	9.7	1.4/1.5	2.0
SBAPPN10a	10.1/11.7	5.8/11.6	5.0/11.6	647/153	8.8	1.2/1.3	2.9
SBAPPN10b	10.0/11.5	5.8/11.6	5.0/11.6	781/147	8.9	1.6/1.7	2.2
SBAPPN30a	10.0/11.5	5.8/11.6	5.0/11.6	420/109	8.0	0.8/0.9	3.1
SBAPPN30b	10.0/11.5	5.8/11.6	5.0/11.6	541/106	8.8	1.0/1.1	2.3

Description of symbol: $d_{(hkl)}$ = interplanar spacing, $a_{(hkl)}$ = lattice parameter, S_{BET} = specific surface area, D_p = pore diameter, V_{BJH} = pore volume, V_t = total pore volume, Wt = wall thickness, estimated from the SAXS data and pore diameter ($a_{(100)} - D_p$).

occupying the surface of the silica matrix. Higher encapsulation times may increase the entrapment of papain inside the mesopores, resulting in lower Scale_q^4 values.

3.3. N_2 adsorption-desorption analysis

Fig. 5 shows the physisorption isotherms (A and C) and pore size distribution (B and D) for pure SBA-15 and SBAPPN biocomposites. All samples exhibited isotherms of type IV with hysteresis loop of type H1, according to the IUPAC classification [45], which are typical of ordered mesoporous silica such as SBA-15.

Textural parameters, such as specific surface area (S_{BET}), pore diameter (D_{pore}), pore volume (V_{BJH}), total pore volume (V_t), C-values and wall thickness (W_t), were calculated using $W_t = a_{(100)} - D_{pore}$ equation [46], of SBA-15 and SBAPPN biocomposites, are presented in Table 1. All biocomposites presented slight lower values of superficial area and pore volume (V_{BJH} and V_t) compared to SBA-15 due to papain inside of the mesopores, which were more evident in samples prepared using a time of stirring of 60 min and samples with higher papain content (30 wt%), corroborating with the SAXS results. The C-values (Table 1) of the biocomposites decreased slightly compared to pure silica probably due to the decrease in free hydroxyls due to their interaction with papain molecules or due to incorporation of these molecules within the mesopores [47].

3.3. SEM micrographs

Figs. 6 and 7 present the SEM images of the pure ordered mesoporous silica and SBAPPN biocomposites, respectively. As shown in Fig. 6, SBA-15 exhibited a typical interconnected rod-like morphology. For both SBAPPN biocomposites, the SEM micrographs (Fig. 7) showed no significant morphological change, suggesting that the bulk structure of SBA-15 was retained after the papain incorporation.

3.4. FTIR spectroscopy

FTIR spectroscopy was used to examine the changes in the structure of silica and papain when the biocomposites were formed. Fig. 8 shows FTIR spectra of SBA-15, papain and the biocomposites. The FTIR spectrum of SBA-15 exhibits a band at 3390 cm^{-1} which is assigned to surface hydroxyl group (νO-H) of silanol groups (Si–OH) and of adsorbed water. A weak band at 962 cm^{-1} (νSiO) is detected. The O–H bending vibration of physically adsorbed water molecules appears at 1635 cm^{-1} and the typical vibrations of siloxanes groups appear in the 1200-500 cm^{-1} range. The strong band at 1070 cm^{-1} was attributed to asymmetric stretching vibration of siloxane groups (Si–O–Si). The symmetric stretching vibration from SiO bonds appears at 795 cm^{-1} and the bending vibration from Si–O–Si at 436 cm^{-1} [42,48]. Papain FTIR

Table 2
Values of the parameters used to fit the SAXS experimental data.

Sample/Fitting Parameter	SBA-15	SBAPPN10a	SBAPPN10b	SBAPPN30a	SBAPPN30b
Scale (10^3)	10.850 ± 0.079	3.888 ± 0.057	7.13 ± 0.11	4.14 ± 0.13	6.68 ± 0.15
Radius (Å)	51.15 ± 0.15	48.68 ± 0.27	49.25 ± 0.29	47.57 ± 0.52	48.50 ± 0.37
R_outer (Å)	67.14 ± 0.14	69.51 ± 0.27	68.38 ± 0.29	69.72 ± 0.54	69.82 ± 0.39
Backgr (10^{-3})	17.88 ± 0.49	4.91 ± 0.20	9.91 ± 0.36	0	2.43 ± 0.28
Scale_q^4	0	121.2 ± 9.4	241 ± 18	445 ± 33	1023 ± 45

Parameter description: Scale = global scale factor, Radius = radius of the mesopore, R_outer = corresponds to the parameter Radius added to the wall thickness of the amorphous silica, Backgr = constant background, Scale_q^4 = scale factor for the scattering at low q, which is proportional to q^4. a = 60 min and b = 30 min.

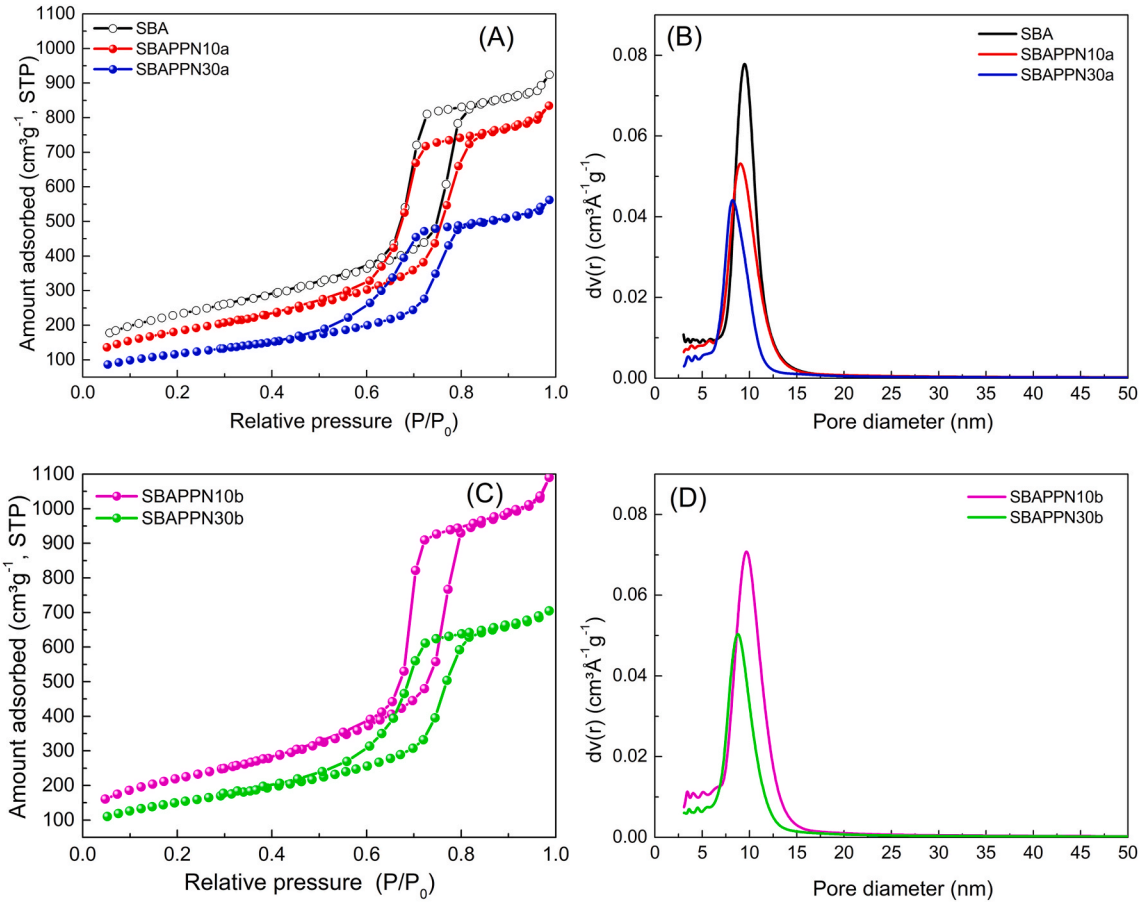

Fig. 5. (A) and (C) Adsorption-desorption isotherms of SBA-15 and SBAPPN materials. (B) and (D) pore diameter of SBA-15 and SBAPPN biocomposites.

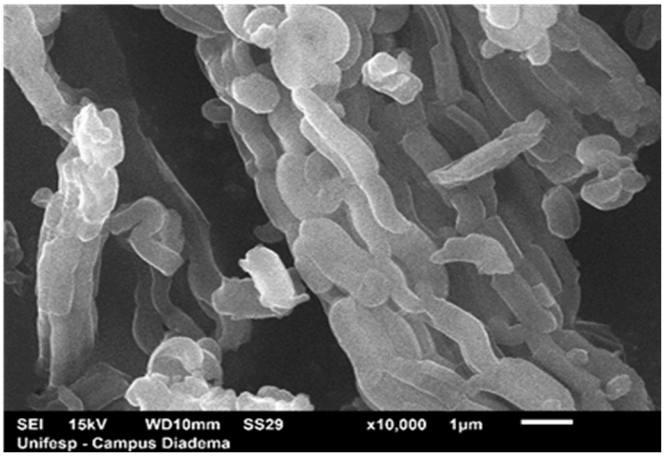

Fig. 6. SEM image of SBA-15.

spectrum displays a band at 3263 cm^{-1} and it was assigned to N–H stretching, coinciding with the broad absorption band of O–H. The band at 2924 cm^{-1} is typical of $–CH_2$ asymmetric stretching and the bands at 1640 cm^{-1} and 1394 cm^{-1} attributed to C═O asymmetric and symmetric stretching, respectively, corresponding to amide I band. The band at 1529 cm^{-1} is attributed to vibrations on the plane of the N–H bond and to the C–N bending vibration, related to amide II [22,49,50]. All biocomposites exhibit the typical vibrations of SBA-15 and some vibration bands of papain, such as amide I and II bands. The silanol groups (Si–OH) of SBA-15 can interact with the amide groups of papain, forming hydrogen bonds [51]. Because the characteristic peaks of papain amide groups at 1394 cm^{-1}, 1529 cm^{-1} and 1640 cm^{-1} did not alter significantly in the SBAPPN biocomposites, the intermolecular interaction between silica and protein is likely weak.

3.5. Thermal analysis

TG/DSC curves of papain and SBA-15 are presented in Fig. 9. TG curve of papain shows three events of weight loss. The first corresponds to release of water molecules (5%), in the temperature range 35–140 °C, presenting an endothermic peak in DSC curve. The thermal decomposition of papain (2nd and 3rd steps), in the temperature range of 140–445 °C (60%) and 445–900 °C (33%), respectively, which are accompanied by two exothermic peaks in the DSC curve [52]. It is worth mentioning that, around 600 °C, the decomposition products of papain were eliminated, and no residue remained. TG curve of pristine SBA-15 shows an initial weight loss (1.5%) from 35 to 157 °C that corresponds to the evaporation of physically adsorbed water, which is associated to a DSC endothermic peak centered at 96 °C. The second step of weight loss (4.3%), in temperature range of 157–900 °C, was attributed to the dehydroxylation of surface silanols [53].

Fig. 10 shows TG/DSC curves of SBAPPN biocomposites. Comparing the TG curves of these biocomposites and free papain, it was noted that the onset temperature for papain thermal decomposition in the biocomposites was higher (around 270 °C) than the pure papain (242 °C) and the final temperature of papain thermal decomposition was higher for SBAPPN biocomposites (above 700 °C) than for pure papain (around 600 °C), indicating that the immobilization of papain enzyme into SBA-15 matrix protected the enzyme against thermal decomposition, corroborating that immobilization might be a good alternative to protect enzymes from physical agents [54]. The time of stirring (30 or 60 min)

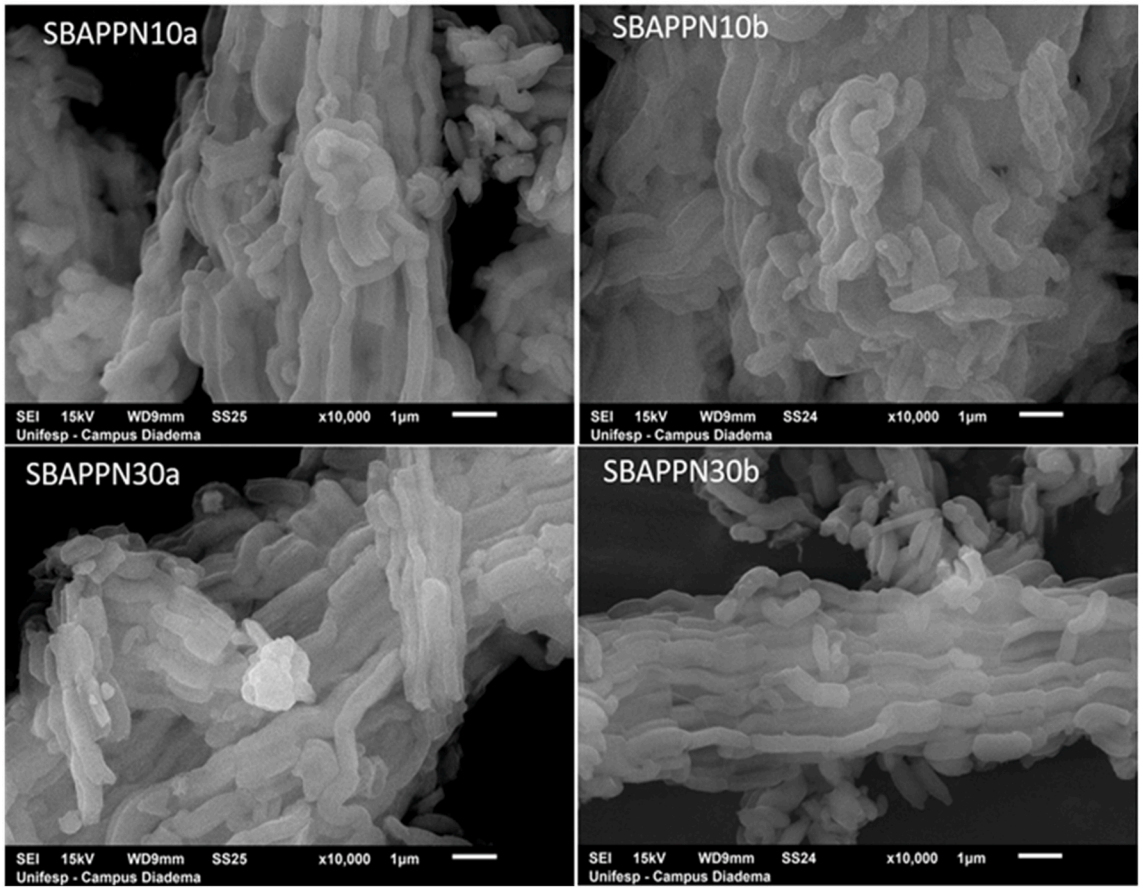

Fig. 7. SEM images of SBAPPN biocomposites.

used for biocomposites preparation did not significantly influence in the onset temperature. Although the samples prepared with 10 wt% of papain have shown higher protection when compared with the ones prepared with higher papain content (30 wt%), which can be related to the presence of papain outside the mesoporosity.

For all biocomposites, the TG curves (Fig. 10 and Table 3) show three weight loss events, similar to papain curve, however, in different temperature ranges. For the SBAPPN10 biocomposites, the first event (35–165 °C), with weight loss ranging between 3 and 5%, and endothermic peak in DSC, corresponds to the loss of physically adsorbed water. The second (155–510 °C) and third (510–900 °C) ones were assigned to thermal decomposition of papain and elimination of silanol groups on silica particles which are condensed to siloxanes (total weight loss around 12%), with exothermic peaks in DSC, like the papain one. For the SBAPPN30 biocomposites, the first event (35–145 °C), with weight loss at 2.8%, corresponds to the loss of physically adsorbed water (endothermic peak in DSC) and the other events which occurs in the temperature ranges of 145–490 °C (second event) and 490–900 °C (third event) were attributed to papain thermal decomposition and silanol groups elimination (total weight loss close 27%), both events correspond to exothermic peaks in the DSC. The lowest papain thermal decomposition for the SBAPPN30 biocomposites is indicative of papain outside the mesopores, which is corroborated by SAXS. Considering that the papain contains 5 wt% of adsorbed water and the nominal content of papain in the biocomposites was 10 and 30 wt%, we can consider that the papain content obtained by TG curves, for the biocomposites, is similar to the nominal content of used papain (Table 3).

Elemental analysis (CHNS) was performed for the pure papain and the biocomposites (SBAPPN). The papain content in the biocomposite samples was estimated by the percentage of carbon and nitrogen in each sample, because these elements are the majoritarian components papain, using pure papain as a reference. Elemental analysis for the pure papain revealed the presence of carbon and nitrogen, in a concentration of 40.5 wt% and 12.2 wt%, respectively. By these results and the obtained results for the biocomposites (SBAPPN10a (C = 6.4 wt% and N = 1.9 wt%), SBAPPN30a (C = 11.3 wt% and N = 3.4 wt%), SBAPPN10b (C = 6.1 wt% and N = 1.8 wt%), and SBAPPN30b (C = 10.9 wt% and N = 3.3 wt%) the papain content in the SBAPPN biocomposites was estimated, which corresponds to a content around 16 wt%, 28 wt%, 15 wt% and 27 wt%, receptively, for SBAPPN10a, SBAPPN30a, SBAPPN10b and SBAPPN30b. These results revealed that the content of papain obtained by elemental analysis is close to the nominal content, especially for the samples with a content of 30 wt%.

3.6. Enzyme activity assay

One of the highest challenges as working with bioactive compounds is to guarantee that such compounds maintain its features such as the chemical structure and biological activity. For enzymes, it is especially true, because its usefulness in several fields is related to capability in transforming substrates in products, normally with low energy consumption.

In this work, papain was in contact with SBA-15, a mesoporous silica, able to entrap molecules inside its pores, aiming the controlled release and protect against physical or chemical destabilization factors. The assays performed for the characterization of SBAPPN composites were able to confirm that papain has occupied the mesopores of SBA-15 and, likely, that some protein aggregates are in the surface of the silica matrix. Despite the presence of papain entrapped in silica, the previous assays are not able to inform if papain had maintained its biological activity. In order to assess the preservation of enzymatic activity in the composites, SBAPPN was in contact with its specific substrate BAPA.

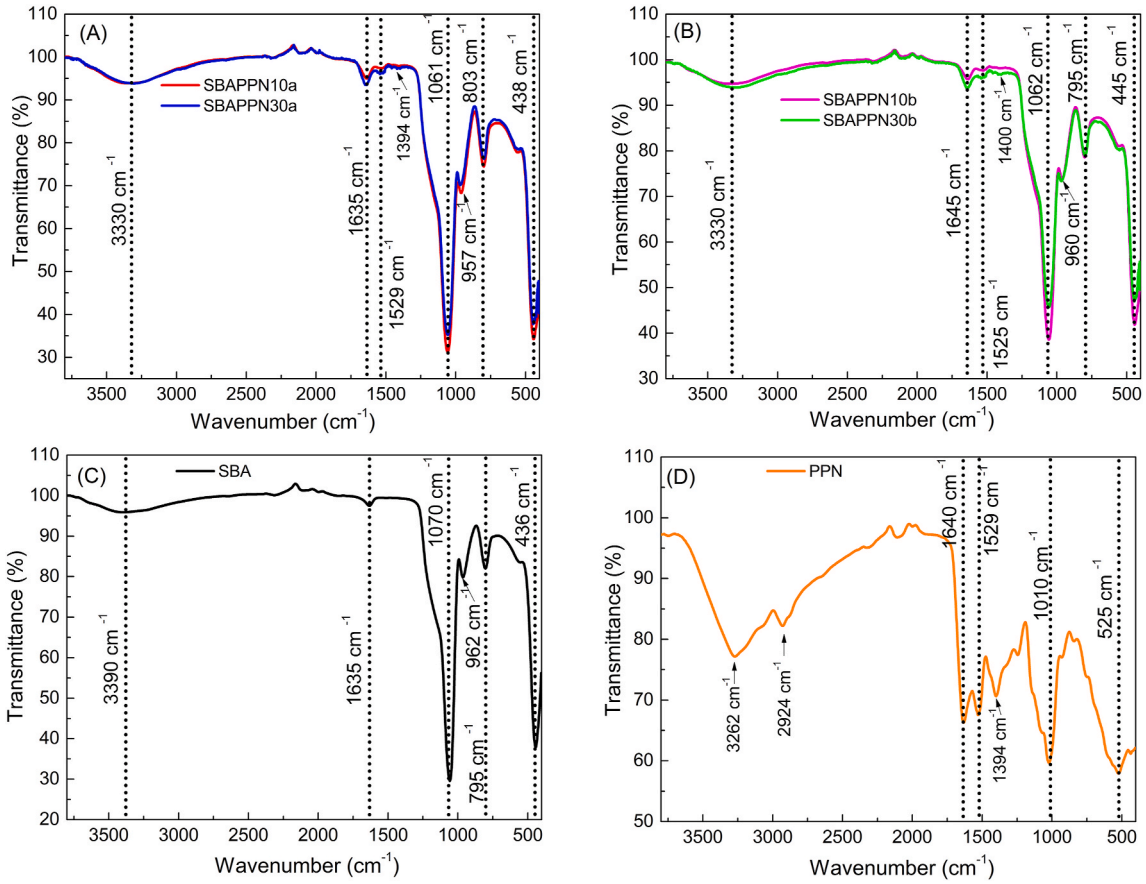

Fig. 8. FTIR spectra of SBA-15, papain and SBAPPN biocomposites.

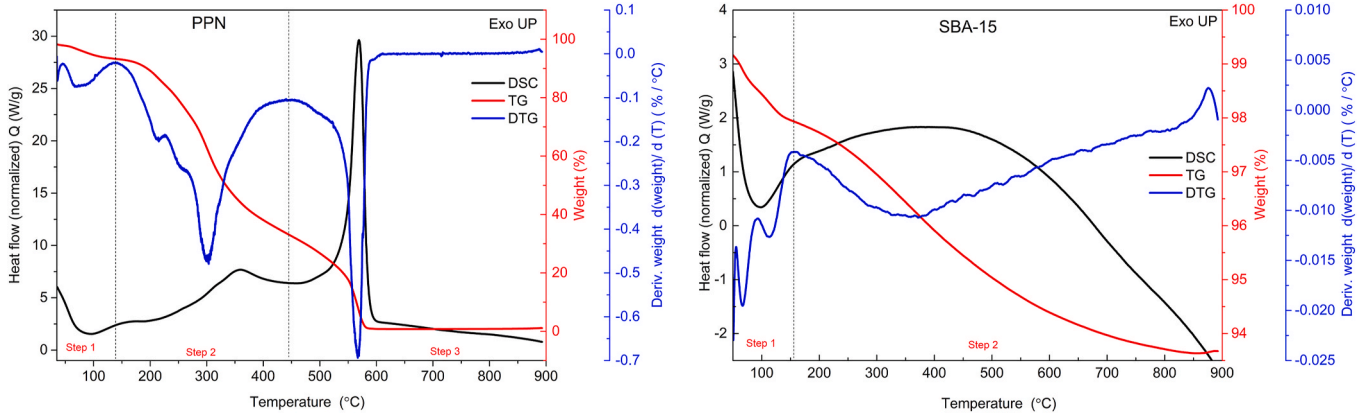

Fig. 9. TG/DSC curves of pure SBA-15 and papain.

Fig. 11A shows the analytical curve for papain activity found for eight different concentrations of papain ranging from 0.0090 to 0.1090 mg mL^{-1} ($R^2 = 0.982$, $y = 0.0531x + 0.0002$). A concentration of 0.0909 mg mL^{-1} was chosen to perform the enzymatic activity assay for SBAPPN materials, however those with 10% papain (SBAPPN10) reached correlation coefficients lower than 0.90, specially SBAPPN10b ($R2 = 0.6351$) not allowing to build valid curve between absorbances and time, whereas for SBAPPN10a, despite the low value ($R2 = 0.8607$), the BAPA conversion rate was calculated to compare with SBAPPN30 composites. PPN solution in the same concentration (0.0909 mg mL^{-1}) was used as control reaching at 105.89% of PPN relative biological activity. For each sample, the linear equation was determined, and the angular coefficient (BAPA conversion rate) was applied in the analytical curve for papain activity. Data of linear correlation, BAPA conversion rate, determined PPN concentration and relative biological activity are shown in Fig. 11C.

As shown in Fig. 11D, it was found a significant difference between SBAPPN composites as ANOVA One-way was applied to compare the PPN activity (p-value = 0.034). Tukey test unveiled to exist difference between SBAPPN30b and SBAPPN10a, belonging to different groups, whereas for SBAPPN30 composites no difference was determined. Despite that, the higher enzymatic activity for SBAPPN30b (89.78%) in relation to SBAPPN30a (87.01%) may be related to the slightly higher presence of exposed papain in SBA-15, corroborating with SAXS, NAI, and TG data, which show that for the half-hour of agitation, papain gets less into the SBA-15 mesopores, making it more easily available to

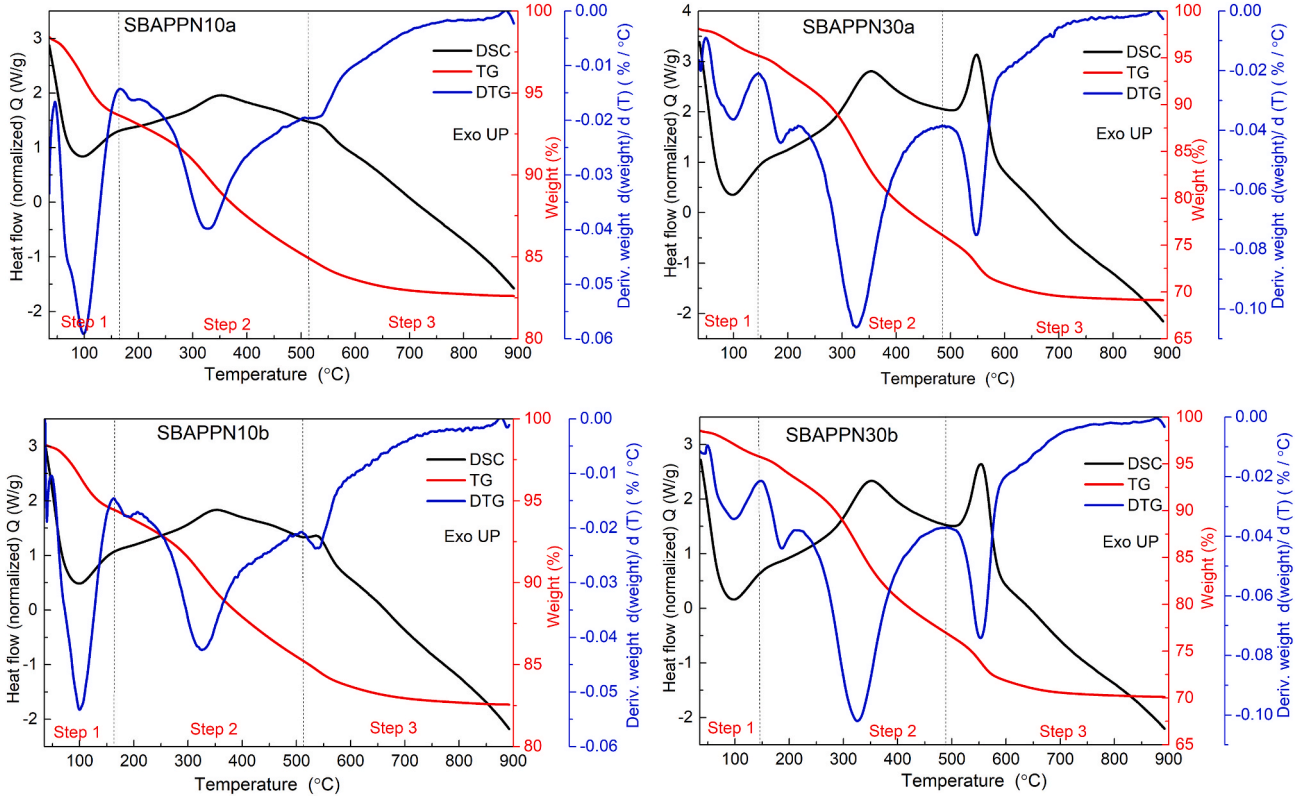

Fig. 10. TG/DSC curves of SBAPPN biocomposites.

Table 3
DSC and TGA thermal analysis results of papain (PPN), pure SBA-15 and SBAPPN biocomposites.

Samples	Step 1 *35–140 °C					Step 2 *140–445 °C					Step 3 *445–900 °C					Residue at 900 °C
	Δw (%)	T_{onset} (°C)	T_{peak} DTG (°C)	T_{peak} DSC (°C)	ΔH (J g^{-1})	Δw (%)	T_{onset} (°C)	T_{peak} DTG (°C)	T_{peak} DSC (°C)	ΔH (J g^{-1})	Δw (%)	T_{onset} (°C)	T_{peak} DTG (°C)	T_{peak} DSC (°C)	ΔH (J g^{-1})	Δw (%)
*PPN	5.0	59	80	83	1242	60.0	242	213 255 301	359	1640	33	547	567	569	4693	2
SBA-15	1.5	41	67 113	96	1213	4.3	260	350	507	5014	–	–	–			94.2
SBAPPN10a	4.7	67	98	94	657	6.7	275	188 327	350	226	4.4	429	540	540	281	84.2
SBAPPN10b	3.9	72	100	96	753	7.3	276	189 326	350	318	4.7	438	543	542	296	84.1
SBAPPN30a	2.8	72	96	97	892	18.7	270	184 326	349	730	7.4	531	547	549	533	71.1
SBAPPN30b	2.8	69	95	95	753	18.3	266	185 325	350	752	7.7	533	552	556	496	71.2

T = temperature, Δw = weight loss, ΔH = enthalpy (normalized).

interact with BAPA. On the other hand, these values of biological activity are close to free papain if considered that the free papain is totally available to interact with specific substrate whereas papain entrapped in silica depends on that BAPA in solution get closer and into the silica to interact with papain. Furthermore, in the preparation of SBAPPN, only a part of papain put to interact with silica might have been entrapped by. This suggests that the papain in silica continued being active, and even with a fraction of papain entrapped the activity was kept about 87–89%. The same was found by Bhange et al. [55] for immobilization of bile salt hydrolase in SBA-15 since the enzyme kept its activity and showed better stability as exposed to high temperatures and extremes of pH. Also, Fan et al. [56] entrapped in SBA-15 by absorption method an enzyme esterase (Est648), from a gene expressed in Escherichia coli, recovering an activity about 81.3% in optimized conditions, corroborating the findings of this work.

3.7. Leaching of PPN from SBAPPN composites

Aiming to elucidate if the SBAPPN biocomposite is kept in water or tends to dissociate releasing PPN, the samples of SBAPPN30a was assessed for leaching up to 8 h under stirring in deionized water at room temperature. This experiment can evaluate how much PPN is released from the composite to the aqueous medium and consequently could exert its biological activity as a free molecule in solution. Thus, SBA-15 could play two different roles, one related to enzyme protection due to the entrapment, and the other related to the control of the PPN release

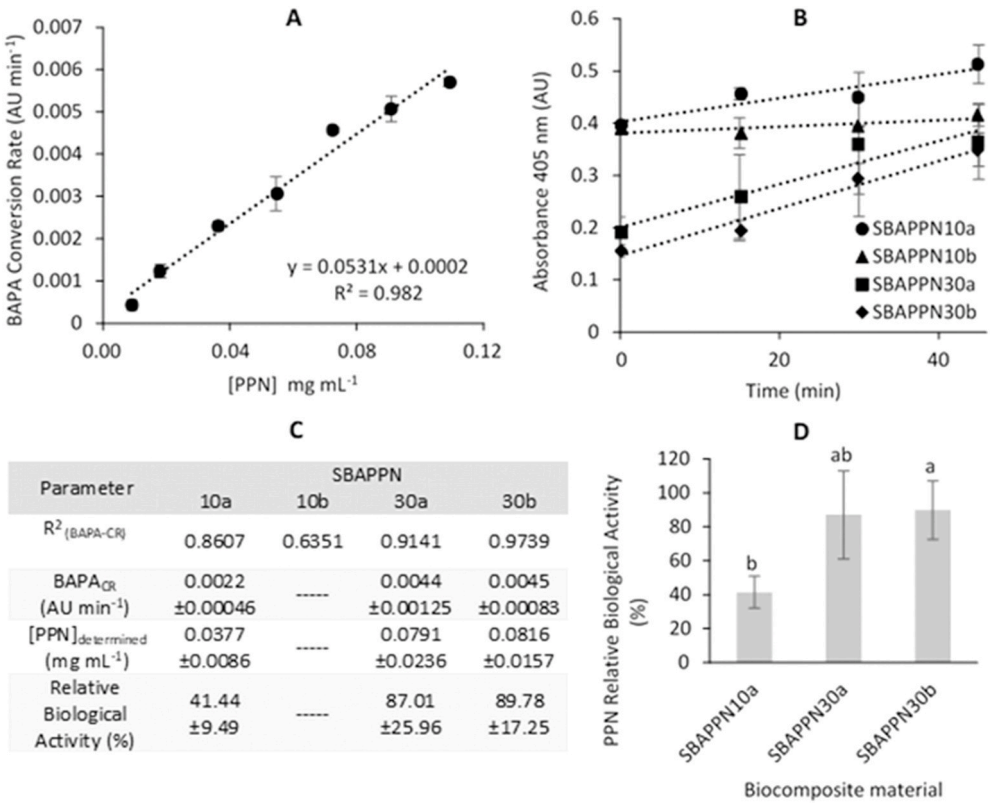

Parameter	SBAPPN 10a	10b	30a	30b
$R^2_{(BAPA-CR)}$	0.8607	0.6351	0.9141	0.9739
$BAPA_{CR}$ (AU min^{-1})	0.0022 ±0.00046	-----	0.0044 ±0.00125	0.0045 ±0.00083
$[PPN]_{determined}$ (mg mL^{-1})	0.0377 ±0.0086	-----	0.0791 ±0.0236	0.0816 ±0.0157
Relative Biological Activity (%)	41.44 ±9.49	-----	87.01 ±25.96	89.78 ±17.25

Fig. 11. Determination of papain activity through BAPA substrate specific reaction. A-analytical curve of papain activity; B- BAPA conversion rate at 0.0909 mg mL^{-1} PPN in SBAPPN biocomposites; C- data of PPN activity analysis; D- PPN relative biological activity. In D, ANOVA One-way unveils significant difference between samples (p-value = 0.034); equal letters represent values in a same group as Tukey test was applied.

from the composite to the aqueous medium.

To quantify the PPN leached to aqueous medium, an analytical curve for PPN in 230 nm was obtained and expressed by the equation [PPN]= (Abs230nm + 0.0159)/2.804 (r^2 = 0.9999). The equation was used to calculate directly the PPN concentration in samples. The values determined of PPN concentration were related to theoretical PPN concentration in sample and percentual recovery value stablished. Fig. 12 shows the profile of PPN leached up to 8 h.

The statistical analysis from data of PPN leaching from SBAPPN30a indicates that there is significant difference among the amounts of PPN leaching in the four times investigated (p = 0.0005). However, Tukey test for grouping samples considering a 95% of confidence interval shows difference just to samples at 8 h (53.5% of PPN leached),

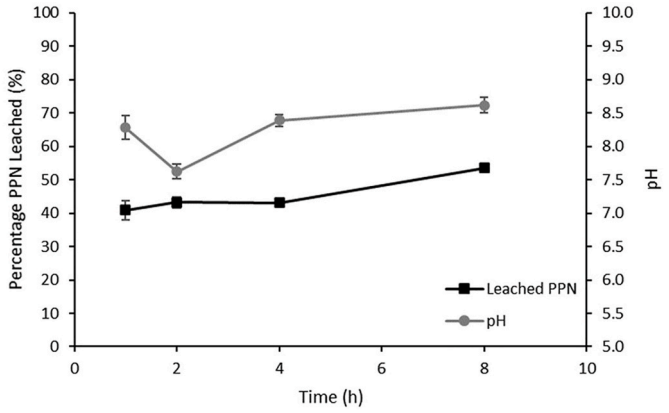

Fig. 12. Leaching of PPN from SBAPPN30a in purified water under stirring at room temperature. The pH values were determined after filtration through a nylon membrane 0.22 μm pore.

indicating that in the first 4 h the samples leaches amounts of PPN very close (around 43% of leached PPN). This finding unveils that since the first hour the PPN adsorbed on SBA-15 surface was rapidly dissolved to water medium, which was prevalent up to 4 h. On the other hand, at 8 h assay, the amount of PPN leached was increased in 11%, suggesting that a fraction of PPN more intimately linked with SBA-15 starts to gain the aqueous medium in amounts sufficient to be recorded. These data showed that at least 57% of the PPN in the biocomposite SBAPPN30a is more intensively associated with SBA-15 and could be released slowly, extending the time of enzyme action in a therapeutic system.

The data of PPN leaching analysed together the data of biological activity indicate that PPN present in SBAPPN30a biocomposites maintain its activity even as entrapped in the SBA-15 mesopores, since the activity test was carried out just for 45 min recording about 87% of biological activity, while less than 45% of PPN was found in solution within the first hour. In this sense, at least 42% of activity might be attributed to PPN still entrapped into silica mesopores, demonstrating that biological activity is maintained even in this condition.

Considering the therapeutic use of PPN, the results indicate that SBAPPN biocomposites could be used as immediate as prolonged action, what would be useful in the treatment of ulcerative process to the skin, gastrointestinal tract, or other biological surface, or as a permeation enhancer for the skin in cosmetic and pharmaceutic bioactives.

Regarding pH of aqueous medium, after leaching experiment, the values ranging from 7.62 (4 h) to 8.62 (8 h). This values are different of those obtained during the several SBAPPN preparation (pH 4.94–5.06). These values were expected since solutions of papain in water shows pH around 5.1–5.3, and SBA-15 dispersed in water shows pH of 5.3. The higher pH values after leaching assays might be attributed for slowly SBA-15 dissolution. In fact, SBA-15, as other silica compounds, may dissolve so slowly in water, becomes the medium weakly alkaline [57, 58].

3.8. Cytotoxicity assays

In order to mimic the *in vivo* environment, 3D *in vitro* models without scaffolds could be produced, such as the spheroid model here employed, to evaluated proteolytic enzymes, as papain, which presents an anoikis effect [59]. This effect where the cell death process could be caused by cell detachment, which activates apoptotic mechanisms instead of necrosis associated with inflammatory responses, could lead to false results regarding the cytotoxicity of papain [60].

Cell culture on flat surfaces (2D models) was important to understand molecular principles in cell biology. However, these culture conditions do not accurately reflect the *in vivo* situation like correct tissue architecture, cell-cell contact and cell-matrix interactions. 3D models are promising candidates for improved preclinical models because they represent appropriate physiological systems and are suited to perform cell-based drug screening or to evaluate potential therapeutic molecules [61].

We performed the test using the vital dyes: MTT (formazan) and PrestoBlue™ (resazurin). The first one is widely employed at 2D cytotoxicity assays and is a reliable method. The cell viability is assessed by measuring the mitochondrial function, which reduces the tetrazolium salt to the purple formazan by cellular dehydrogenase enzymes on living cells [62]. The second one is a fluorometric method to estimate the number of viable cells by measuring the reduction of resazurin into resorufin [63].

The cytotoxicity in spheroids of SBA-15 ordered mesoporous silica materials containing papain (Fig. 13) showed that papain do not present cytotoxicity (100% cell viability) but presented a statistically significant difference (p-value = 0.0422) between the MTT and PrestoBlue™ vital dye assays, when using the Sidak's multiple comparisons test.

The composite formed by SBA-15 and papain (79 and 65% cell viability) and SBA-15 alone seems to induce cytotoxicity (50 and 47% cell viability), an effect that was not observed by Vieira et al. [43]. This could be explained by the diversity of the methods, as at the previous paper the authors used a 2D model to assess the cytotoxicity of SBA-15 and the use of a different viability cell dye, Neutral Red Uptake assay, that relies on the intracellular accumulation of the dye in cellular lysosomes via active transport instead of the enzymatic conversion of the dye in mitochondria and endoplasmic reticulum as formazan or just in mitochondria as resazurin [64]. In general, the results obtained with MTT assay depend on metabolic rate and on the number of mitochondria result in many known interferences [64].

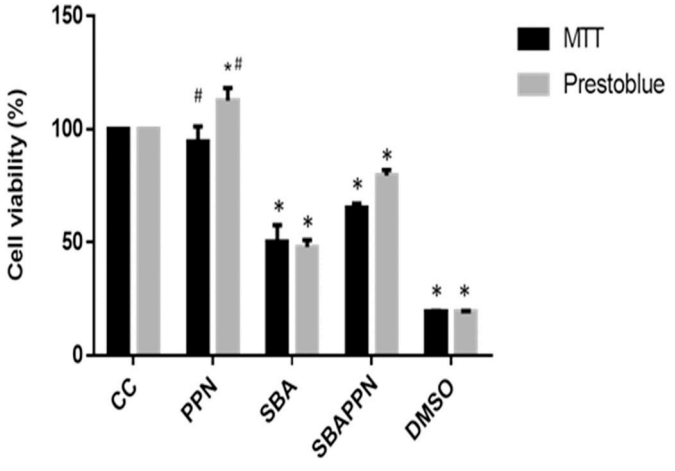

Fig. 13. Cytotoxicity assay using Balb/c 3T3 cells in a Bio-Assembler™ System and MTT and PrestoBlue™ as vital dyes. CC (cell control), SBA (0.7 mg mL^{-1}), SBAPPN biocomposites (5 mg mL^{-1}), PPN (0.216 mg mL^{-1}) and DMSO (200 mg mL^{-1}). ANOVA One-way unveils significant difference between samples where *p < 0.05 sample vs. cell control as Tukey test was applied. # represents a comparison of results by one-way ANOVA and the Sidak's multiple comparisons test to evaluate the difference between the samples when comparing the two viability dye assays.

All the samples and the positive control showed a difference statistically significant (Tukey's multiple comparisons test) when compared with the cell control, for both cell viability evaluation assays, presenting p-values of CC vs. PPN (0.0453); CC vs. SBA (<0.0001), CC vs. SBA-PPN (0.0058) and CC vs. DMSO (<0.0001) for PrestoBlue™ assay and CC vs. SBA (pvalue = 0.0006), CC vs. SBA-PPN (0.0037) and CC vs. DMSO (<0.0001) when comparing the results for MTT assay.

Di Pasqua et al. [65] also discussed that the cytotoxic chemical origins of the mesoporous silica are unknown, although the exposed surface area of the particle appears to be an important factor in causing cell death. In addition, we also suppose that the presence of the SBA-15, a highly absorptive material, could affect the cells organization on the spheroid form, blocking the dye permeation and consequently limiting the amount of the dye conversion in living cells. This hypothesis must be further clarified.

Corazza et al. [29] found that papain, even in a triple co-culture presents cytotoxicity, mostly due to the anoikis effect. The results here presented for papain could be explained based at the structure of the spheroids. If the cells form a tight spheroid, viability dyes could not penetrate it leading to low responses. On the other hand, if the studied chemical disrupts tight cell-cell interactions of the spheroids this will result in augmented vital dye activity. However, cytostatic chemicals, which only affect cell proliferation without interfering with cell-cell contacts leads to an exceptionally low vital dye activity. In this context our results corroborated that papain acts as a disruptive substance instead of a cytostatic one, where DMSO (our positive control – 26 and 30% cell viability) could be considered a real cytotoxic chemical as fewer cells in a tight spheroid simply reduce less vital dye and SBA-15 do not present a cytotoxicity or even a disruptive mechanism.

4. Conclusions

From the IFT analysis of SAXS data of pure papain in solution, we concluded that the dispersed papain is a globular and slightly elongated protein, likely dimeric, with a maximum size of ~6.0 nm and a radius of gyration of ~2.0 nm. The protein molecular weight estimated from the forward scattering is reasonable compared to the expected one, indicating that the sample is quite monodisperse. This is corroborated by DLS analysis, which showed the presence of only a few large protein aggregates (with mean diameter ~60.0 nm). In terms of volume and number, most of the papain particles have an average hydrodynamic diameter of ~4.0 nm. Simulations with CRYSOL and HYDROPO software highlighted the existence of good agreement between all SAXS and DLS observations and the crystallographic structure of the protein. The predicted hydrodynamic diameter is ~4.7 nm, compatible with DLS observations. In addition, the simulated radius of gyration and the longest papain length are, respectively, ~1.7 and ~6.0 nm, in agreement with SAXS results.

The SAXS results also indicated that the papain was incorporated into the SBA-15 mesopores, whereas the aggregates are likely in the surface of the silica matrix. The biocomposites (SBA-15:papain) showed high thermal stability when compared to pure papain and are quite promising for biomedical applications. It was observed that the amount of papain (10 and 30 wt%) used to prepare the biocomposites influences the papain thermal stability. It was also observed that the reaction time may influence the amount of papain loaded into the SBA-15 mesopores. Protein aggregates on the surface of the silica matrix also was evidenced. Papain entrapped in SBA-15 mesoporous silica had its biological activity maintained since it was achieved about 89% activity to the composite with the best performance (SBAPPN30b). These results corroborate the ability to SBA-15 in carrying biological molecules, preserving their biological function, what is extremely important when it is looked for the use of those biocomposites in products for health and wellness or other fields of industrial interest.

The leaching results indicated that SBAPPN biocomposites can be used as immediate as prolonged action, considering the therapeutic use of PPN, which would be useful in the treatment of ulcerative process to the skin, gastrointestinal tract, or other biological surface, or as a permeation enhancer for the skin in cosmetic and pharmaceutic bioactives.

Furthermore, no important cytotoxicity was attributed to papain when a 3D system was employed; showing that papain, when entrapped in SBA-15, in addition to maintaining the biological activity, also do no present cytotoxicity. The results also showed that the 3D cell culture system is better suited for biocomposites that present a cell disruption mechanism.

Declaration of competing interest

The authors declare that they have no known competing financial interests or personal relationships that could have appeared to influence the work reported in this paper.

Acknowledgments

We thank Dr. A.C.F. Silveira and Mr. T.M. Germano from LCr-IF-USP for SAXS measurements and BSc C.M. Fukumoto, MSc. R.M. da Silva and Dr. R. Rodrigues from NIPE-UNIFESP for SEM, EDS and NAI measurements. This work was supported by the FAPESP (processes numbers 17/17844-8, 19/08582-5, 2016/22916-5, 2017/26618-1), and CAPES (Education Ministry) (process number 23038.000776/201754) via the projects of the National Institute for Science and Technology on Organic Electronics (INEO). M.C.A. Fantini is CNPq fellow. P.L.O.F acknowledges grant from FAPESP (process number 2019/12301-1 and 2020/13204-7).

References

[1] A.C. Storer, R. Ménard, Handbook of Proteolytic Enzymes 2, 2013, pp. 1858–1861, https://doi.org/10.1016/B978-0-12-382219-2.00418-X.
[2] J. He, M. Wu, X. Feng, X. Shao, W. Cai, RSC Adv. 4 (2014) 13304–13312, https://doi.org/10.1039/c3ra47346e.
[3] Y.-J. Gu, M.-L. Zhu, Y.-L. Li, C.-H. Xiong, Int. J. Biol. Macromol. 112 (2018) 1175–1182, https://doi.org/10.1016/j.ijbiomac.2018.02.079.
[4] M. de L. Meza-Jiménez, P.-R. Pokhrel, R.R.R. de la Torre, G.V. Barbosa-Canovas, H. Hernández-Sánchez, LWT (Lebensm.-Wiss. & Technol.) 109 (2019) 336–341, https://doi.org/10.1016/j.lwt.2019.04.037.
[5] X. Gu, J. Gao, X. Li, Y. Wang, J. Nanosci. Nanotechnol. 18 (2017) 3543–3547, https://doi.org/10.1166/jnn.2018.14695.
[6] E. Shoba, R. Lakra, M.S. Kiran, P.S. Korrapati, RSC Adv. 4 (2014) 60209–60215, https://doi.org/10.1039/c4ra10239h.
[7] K. Atacan, M. Özacar, M. Özacar, Int. J. Biol. Macromol. 109 (2018) 720–731, https://doi.org/10.1016/j.ijbiomac.2017.12.066.
[8] W. Sheng, Y. Xi, L. Zhang, T. Ye, X. Zhao, Int. J. Biol. Macromol. 114 (2018) 143–148, https://doi.org/10.1016/j.ijbiomac.2018.03.088.
[9] H. Dai, S. Ou, Z. Liu, H. Huang, Carbohydr. Polym. 169 (2017) 504–514, https://doi.org/10.1016/j.carbpol.2017.04.057.
[10] H. Wang, D. Shao, IOP Conf. Ser. Mater. Sci. Eng. 397 (2018), 012031, https://doi.org/10.1088/1757-899X/397/1/012031.
[11] L. Zhou, C. Wang, Y. Jiang, J. Gao, Chin. J. Chem. Eng. 21 (2013) 670–675, https://doi.org/10.1016/S1004-9541(13)60528-5.
[12] H.H.P. Yiu, P.A. Wright, N.P. Botting, J. Mol. Catal. Enzym. 15 (2001) 81–92, https://doi.org/10.1016/S1381-1177(01)00011-X.
[13] B. Sahoo, S.K. Sahu, D. Bhattacharya, D. Dhara, P. Pramanik, Colloids Surf. B Biointerfaces 101 (2013) 280–289, https://doi.org/10.1016/j.colsurfb.2012.07.003.
[14] A.A. Homaei, R. Sariri, F. Vianello, R. Stevanato, J. Chem. Biol. 6 (2013) 185–205, https://doi.org/10.1007/s12154-013-0102-9.
[15] Z. Zhou, M. Hartmann, Top. Catal. 55 (2012) 1081–1100, https://doi.org/10.1007/s11244-012-9905-0.
[16] D. Zhao, J. Feng, Q. Huo, N. Melosh, G.H. Fredrickson, B.F. Chmelka, G.D. Stucky, Science 279 (1998) 548–552, https://doi.org/10.1126/science.279.5350.548.
[17] D. Zhao, Q. Huo, J. Feng, B.F. Chmelka, G.D. Stucky, J. Am. Chem. Soc. 120 (1998) 6024–6036, https://doi.org/10.1021/ja974025i.
[18] J.F. Díaz, K.J. Balkus Jr., Enzyme immobilization in MCM-41 molecular sieve, J. Mol. Catal. B Enzym. 2 (1996) 115–126, https://doi.org/10.1016/S1381-1177(96)00017-3.
[19] Y.-C. Yang, J.R. Deka, C.-E. Wu, C.-H. Tsai, D. Saikia, H.-M. Kao, J. Mater. Sci. 52 (2017) 6322–6340, https://doi.org/10.1007/s10853-017-0864-5.
[20] D.P. Serrano, G. Calleja, J.A. Botas, F.J. Gutierrez, Ind. Eng. Chem. Res. 43 (2004) 7010–7018, https://doi.org/10.1021/ie040108d.
[21] A. Galarneau, M. Nader, F. Guenneau, F. Di Renzo, A. Gedeon, J. Phys. Chem. C 111 (2007) 8268–8277, https://doi.org/10.1021/jp068526e.
[22] W. Bian, B. Yan, N. Shi, F. Qiu, L.-L. Lou, B. Qi, S. Liu, Mater. Sci. Eng. C 32 (2012) 364–368, https://doi.org/10.1016/j.msec.2011.11.006.
[23] W. Bian, L.-L. Lou, B. Yan, C. Zhang, S. Wu, S. Liu, Microporous Mesoporous Mater. 143 (2011) 341–347, https://doi.org/10.1016/j.micromeso.2011.03.017.
[24] G.R. Souza, J.R. Molina, R.M. Raphael, M.G. Ozawa, D.J. Stark, C.S. Levin, L. F. Bronk, J.S. Ananta, J. Mandelin, M.-M. Georgescu, J.A. Bankson, J.G. Gelovani, T.C. Killian, W. Arap, R. Pasqualini, Nat. Nanotechnol. 5 (2010) 291–296, https://doi.org/10.1038/nnano.2010.23.
[25] H. Tseng, J.A. Gage, T. Shen, W.L. Haisler, S.K. Neeley, S. Shiao, J. Chen, P. K. Desai, A. Liao, C. Hebel, R.M. Raphael, J.L. Becker, G.R. Souza, Sci. Rep. 5 (2015) 13987, https://doi.org/10.1038/srep13987.
[26] E.P. Barrett, L.G. Joyner, P.P. Halenda, J. Am. Chem. Soc. 73 (1951) 373–380, https://doi.org/10.1021/ja01145a126.
[27] S. Brunauer, P.H. Emmett, E. Teller, J. Am. Chem. Soc. 60 (1938) 309–319, https://doi.org/10.1021/ja01269a023.
[28] C.C. Ferraz, G.H.C. Varca, M.M.D.C. Vila, P.S. Lopes, Int. J. Pharm. Pharmaceut. Sci. 6 (2014) 658–661. ISSN- 0975-1491.
[29] F.G. Corazza, J.V. Ernesto, F.A.N. Nambu, L.R. de Carvalho, V.R. Leite-Silva, G.H. C. Varca, L.A. Calixto, D.P. Vieira, N. Andréo-Filho, P.S. Lopes, J. Drug Deliv. Sci. Technol. 55 (2020) 101413, https://doi.org/10.1016/j.jddst.2019.101413.
[30] B.F. Erlanger, N. Kokowsky, W. Cohen, Arch. Biochem. Biophys. 95 (1961) 271–278, https://doi.org/10.1016/0003-9861(61)90145-X.
[31] G.H.C. Varca, S. Kadlubowski, M. Wolszczak, A.B. Lugão, J.M. Rosiak, P. Ulanski, Int. J. Biol. Macromol. 92 (2016) 654–659, https://doi.org/10.1016/j.ijbiomac.2016.07.070.
[32] F.A.N. Nambu, F.G. Corazza, M.D. Duque, P.S. Lopes, V.R. Leite-Silva, N. Andréo-Filho, Res. J. Pharmaceut. Biol. Chem. Sci. 10 (2019) 112–122, https://doi.org/10.33887/rjpbcs/2019.10.6.14.
[33] W.L. Haisler, D.M. Timm, J.A. Gage, H. Tseng, T.C. Killian, G.R. Souza, Nat. Protoc. 8 (2013) 1940–1949, https://doi.org/10.1038/nprot.2013.125.
[34] D. Svergun, C. Barberato, M.H.J. Koch, J. Appl. Crystallogr. 28 (1995) 768–773, https://doi.org/10.1107/S0021889895007047.
[35] O. Glatter, J. Appl. Crystallogr. 10 (1977) 415–421, https://doi.org/10.1107/S0021889877013879.
[36] C.L.P. Oliveira, M.A. Behrens, J.S. Pedersen, K. Erlacher, D. Otzen, J.S. Pedersen, J. Mol. Biol. 387 (2009) 147–161, https://doi.org/10.1016/j.jmb.2009.01.020.
[37] C.L. P Oliveira, Investigating macromolecular complexes in solution by small angle X-ray scattering, in: A. Chandrasekaran (Ed.), Current Trends in X-Ray Crystallography, InTech, 2011, pp. 367–391, https://doi.org/10.5772/30730.
[38] R.E. Mitchel, I.M. Chaiken, E.L. Smith, J. Biol. Chem. 245 (1970) 3485–3492, https://doi.org/10.1016/S0021-9258(18)62954-0.
[39] I.D. Morrison, E.F. Grabowski, C.A. Herb, Langmuir 1 (1985) 496–501, https://doi.org/10.1021/la00064a016.
[40] A. Ortega, D. Amorós, J.G. de la Torre, Biophys. J. 101 (2011) 892–898, https://doi.org/10.1016/j.bpj.2011.06.046.
[41] A.A.M.L.F. Jardim, R. Bacani, N.S. Gonçalves, M.C.A. Fantini, T.S. Martins, Microporous Mesoporous Mater. 239 (2017) 235–243, https://doi.org/10.1016/j.micromeso.2016.10.009.
[42] A.M.L.F. Jardim, R. Bacani, F.F. Camilo, M.C.A. Fantini, T.S. Martins, Microporous Mesoporous Mater. 228 (2016) 37–44, https://doi.org/10.1016/j.micromeso.2016.03.012.
[43] C.O. Vieira, J.E. Grice, M.S. Roberts, I.N. Haridass, M.D. Dutra, P.S. Lopes, V. R. Leite-Silva, T.S. Martins, Skin pharmacol, Physiol. 32 (2019) 32–42, https://doi.org/10.1159/000491758.
[44] F. Mariano-Neto, J.R. Matos, L.C. Cides da Silva, L.V. Carvalho, K. Scaramuzzi, O. A. Sant'Anna, C.P. Oliveira, M.C.A. Fantini, J. Phys. D Appl. Phys. 47 (2014) 425402, https://doi.org/10.1088/0022-3727/47/42/425402.
[45] K.S.W. Sing, D.H. Everett, R.A.W. Haul, L. Moscou, R.A. Pierotti, J. Rouquérol, T. Siemieniewska, Pure Appl. Chem. 57 (1985) 603–619, https://doi.org/10.1351/pac198557040603.
[46] H. Sanaeishoar, M. Sabbaghan, F. Mohave, Microporous Mesoporous Mater. 217 (2015) 219–224, https://doi.org/10.1016/j.micromeso.2015.06.027.
[47] J.M. Rosenholm, M. Lindén, Chem. Mater. 19 (2007) 5023–5034, https://doi.org/10.1021/cm071289n.
[48] A.G.S. Prado, E.A. Faria, P.M. Padilha, Quim. Nova 28 (2005) 544–547, https://doi.org/10.1590/S0100-40422005000300030.
[49] N. Zou, J. Plank, J. Phys. Chem. Solid. 73 (2012) 1127–1130, https://doi.org/10.1016/j.jpcs.2012.04.016.
[50] S. Peres, E. Armelin, J.A. Moreno-Martínez, C. Alemán, Appl. Surf. Sci. 341 (2015) 75–85, https://doi.org/10.1016/j.apsusc.2015.03.004.
[51] E.S. Manas, Z. Getahun, W.W. Wright, W.F. DeGrado, J.M. Vanderkooi, J. Am. Chem. Soc. 122 (2000) 9883–9890, https://doi.org/10.1021/ja001782z.
[52] Z. Liu, D. Li, H. Dai, H. Huang, J. Mol. Liq. 232 (2017) 449–456, https://doi.org/10.1016/j.molliq.2017.02.100.
[53] R. Purushothaman, J. Porous Mater. 22 (2015) 585–594, https://doi.org/10.1007/s10934-015-9930-z.
[54] J. Rantanen, D. Majda, J. Riikonen, V.-P. Lehto, Acta Mater. 175 (2019) 341–347, https://doi.org/10.1016/j.actamat.2019.06.005.
[55] P. Bhange, N. Sridevi, D.S. Bhange, A. Prabhune, V. Ramaswamy, Int. J. Biol. Macromol. 63 (2014) 218–224, https://doi.org/10.1016/j.ijbiomac.2013.11.008.
[56] X. Fan, W. Liang, Y. Li, H. Li, X. Liu, Microb. Cell Factories 16 (2017) 1382, https://doi.org/10.1186/s12934-017-0767-9.

[57] G. Giovaninni, C.J. Moore, A.J. Hall, H.J. Byrne, V. Gubala, Colloids Surf., B 169 (2018) 242–248, https://doi.org/10.1016/j.colsurfb.2018.04.064.
[58] A. Le-T. Pham, D.L. Sedlak, F.M. Doyle, Appl. Catal., B 126 (2012) 258–264, https://doi.org/10.1016/j.apcatb.2012.07.018.
[59] P. Paoli, E. Giannoni, P. Chiarugi, Biochim. Biophys. Acta Mol. Cell Res. 1833 (2013) 3481–3498, https://doi.org/10.1016/j.bbamcr.2013.06.026.
[60] T. Decker, M.-L. Lohmann-Matthes, J. Immunol. Methods 115 (1988) 61–69, https://doi.org/10.1016/0022-1759(88)90310-9.
[61] A. Walzl, C. Unger, N. Kramer, D. Unterleuthner, M. Scherzer, M. Hengstschläger, D. Schwanzer-Pfeiffer, H. Dolznig, J. Biomol. Screen 19 (2014) 1047–1059, https://doi.org/10.1177/1087057114532352.
[62] T. Mosmann, J. Immunol. Methods 65 (1983) 55–63, https://doi.org/10.1016/0022-1759(83)90303-4.
[63] J. O'Brien, I. Wilson, T. Orton, F. Pognan, Eur. J. Biochem. 267 (2000) 5421–5426, https://doi.org/10.1046/j.1432-1327.2000.01606.x.
[64] A. van Tonder, A.M. Joubert, A.D. Cromarty, BMC Res. Notes 8 (2015) 1–10, https://doi.org/10.1186/s13104-015-1000-8.
[65] A.J. Di Pasqua, K.K. Sharma, Y.-L. Shi, B.B. Toms, W. Ouellette, J.C. Dabrowiak, T. Asefa, J. Inorg. Biochem. 102 (2008) 1416–1423, https://doi.org/10.1016/j.jinorgbio.2007.12.028.